CHAPTER 4

GAS SENSOR AND E–NOSE APPLICATIONS

Currently, gas sensing devices are needed to improve the environmental and safety control of toxic gases. There is a requirement these kinds of sensor for optimizing combustion reactions in the emerging transport industry, and domestic and industrial applications. There are three main groups of gas sensing devices, depending on the supporting technology: solid state, spectroscopic, and optic. The spectroscopic and optic systems are expensive for domestic use and difficult to implement in reduced spaces for example in car engines. Solid state gas sensors gain great advantage in this point as their size is reducible. They are portable, have low power consumption, and are inexpensive. Moreover, they can be used in complex device especially array sensor or e–nose to improve the selectivity of the gas sensor. This chapter discusses firstly fabrication and characterization of gas sensors based on MoO_3 and SnO_2. Then discussion is focused on the sensor array.

4.1 Gas sensors

4.1.1 Introduction

A gas sensor is a device to detect molecules or chemical compounds in gas or vapor. Metal oxide gas sensors typically consist of a metal–oxide semiconducting film coated onto a ceramic substrate, for example alumina, silicon oxide, silicon nitride. Metal oxides used for gas sensors are SnO_2, WO_3, TiO_2, ZnO, ZrO_2, etc. Gas sensors based on SnO_2 were the first commercial MOS which is known as Tagushi gas sensor or Figaro gas sensor, as shown in Fig. 4.1. These sensors are fabricated from SnO_2 with different doping for various applications. Noble metal catalysts such as Pt, Pd, Au, or Cu, are usually used as dopant. These dopants improve the sensitivity and selectivity of MOS. Table 4.1 lists dopants in metal oxide and corresponding target gases. Most often the device also contains a heating element because the operating temperature of MOS is in 200–500°C.

Figure 4.1 Tagushi gas sensors [74]

Table 4.1 Sensing materials and corresponding target gases [76]

Target gas	Additive/Metal oxide
CO	Ag/WO_3, Fe_2O_3, Pd/SnO_2, Pt/SnO_2
CH_4	Pt/SnO_2, Pd/SnO_2
H_2	Pt/SnO_2, Pd/SnO_2, Pt/TiO_2, Nb/TiO_2
NH_3	WO_3, Ag/WO_3, Pt/TiO_3
O_2	In_2O_3, Pd/SnO_2, Nb/TiO_2, TiO_2
C_2H_5OH	Pt/TiO_2, Pd/SnO_2, Nb/TiO_2
NO_2	WO_3, In_2O_3, $LaFeO_3$, Pd/SnO_2, Pt/SnO_2

4.1.2 Fabrication of gas sensor

The sensing layers were deposited on alumina substrates (2 mm x 7 mm or 4 mm x 7 mm) using precipitation method for MoO_3 and SnO_2 thick film and carbothermal reduction method of SnO_2 nanostructures as mentioned in section 3.1. For the precipitation method, MoO_3 or SnO_2 powder was ground to miniaturize the powder size and dispersed in distilled water by sonicating. Alumina substrates were placed at the bottom of a tube and then the suspension was poured into the tube. The light bulb, providing temperature of 70–80°C, was use to evaporate the distilled water. The particles in the suspension gradually precipitated to coat the alumina substrates. After the suspension dried, the substrates were removed from the tube and put into a furnace. The temperature in the furnace was adjusted gradually to increase to 150°C and kept at this temperature for two hours. The thickness of film can be

adjusted by varying the amount of the suspension. This work, MoO_3 and SnO_2 film with thickness of 50 μm and 10 μm, respectively, were fabricated. In addition, gold colloid with concentration of 60 ppm was used to functionalize the layer of SnO_2 nanostructures by dropping technique. The heater for the sensors was made of NiCr wire with diameter of 20 μm by tightly coiling on a 4 mm x 7 mm alumina substrate. The alumina substrate with heater was coupled with another 4 mm x 7 mm alumina substrate on the bottom side and wedged onto an 8–pin IC socket, as depicted in Fig. 4.2. Two IC sockets were coupled together for strength. The ends of NiCr wire were soldered to socket pins below (4 and 5 in Fig. 4.2a). The alumina substrate with sensing element was bound above the heater substrate. Gold wires were glued to the electrodes by gold paste (Ted Pella, Inc., Redding, CA USA) and soldered to socket pins (1 and 8 in Fig. 4.2a).

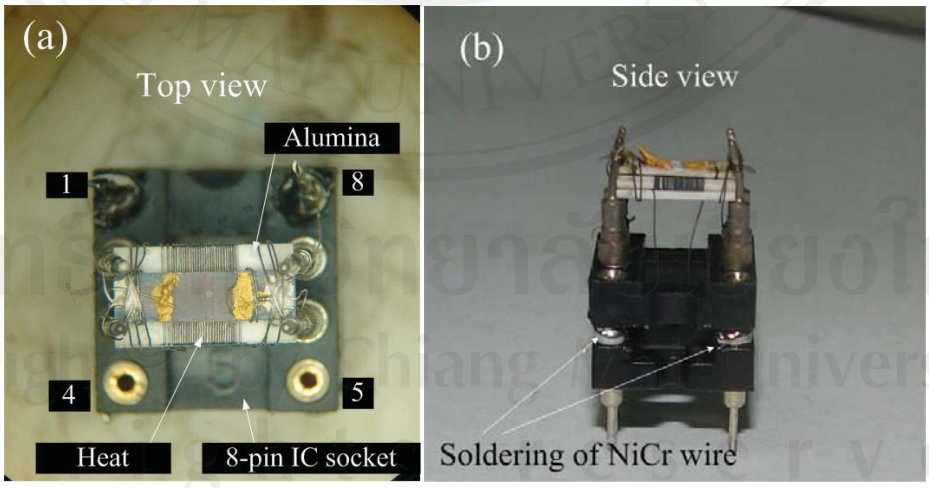

Figure 4.2 Typical developed gas sensor: (a) top view and (b) side view

4.1.3 Ethanol gas sensing properties

The gas sensing properties of the fabricated gas sensors were examined using an ethanol breath simulator (GUTH laboratory Inc., Harrisburg USA) for 50 – 1000 ppm of ethanol vapor concentration which corresponds to the range of alcohol in breath. Ethanol sensing performance was carried out through a gas–confined chamber with inlet and outlet, as shown in Fig. 4.3a. Air flow of 1 ml/min was fed into the chamber as a reference gas through the inlet. The inlet was switched between air and air + ethanol vapor for turning on/off ethanol vapor gas. The gas sensors were exposed to ethanol vapor for 200 seconds over the operating temperature of 200–380°C, measuring by thermocouple placed above the sensing layer. The responses of the fabricated gas sensors to ethanol vapor were measured by using a volt–amperometric technique with 5 volts applied to the sensor, as depicted in Fig. 4.3b.

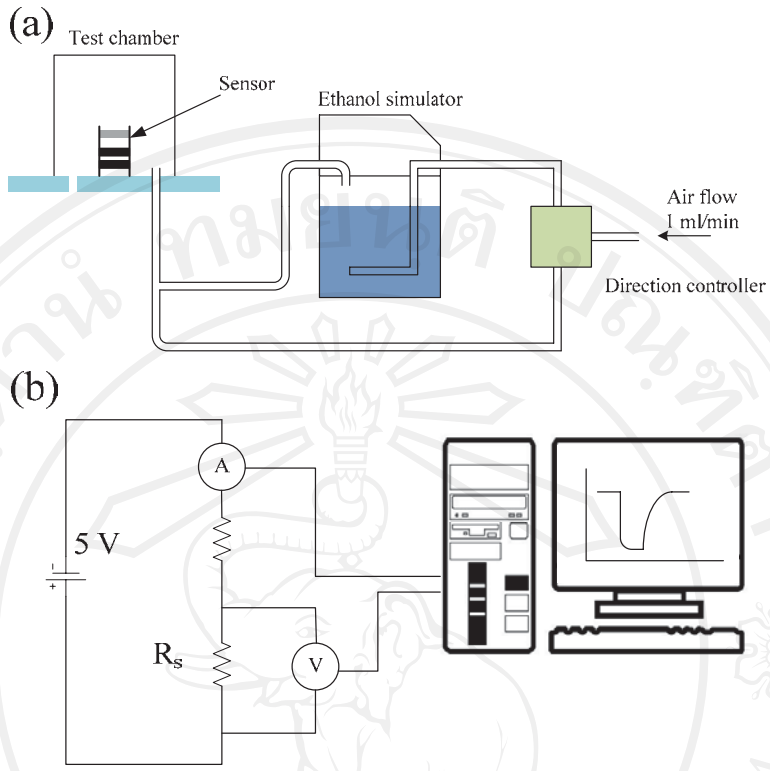

Figure 4.3 Schematic diagram of sensing characteristic measurement: (a) ethanol flowing system and (b) I–V measurement.

4.1.3.1 MoO_3 thick film

The response and recovery curves of sensor based on MoO_3 thick film were shown in Fig. 4.4a for exposing to 200 ppm of ethanol at temperature of 220–340°C. It can be seen the sensing characteristics depend on the operating temperature. The resistance of the sensor decreased as increasing of the operating temperature. Moreover, the response time, and recovery time of the sensor also decreased, in general, when the operating temperature increased. The sensor response gradually increased as increasing of the operating temperature to reach the maximal value of

11.5 at 260°C and gradually decreased with further increasing of the operating temperature, as seen in Fig 4.4b.

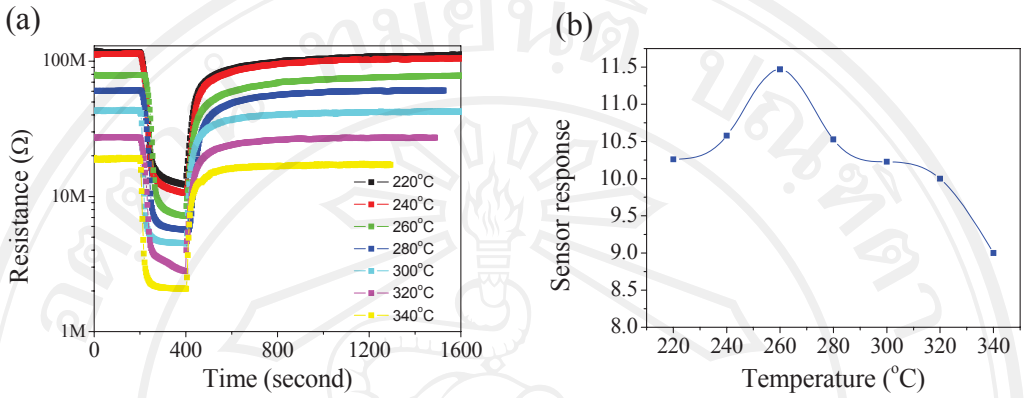

Figure 4.4 (a) Response and recovery curve of MoO_3 thick film sensor and (b) sensor response as a function of temperature for 200 ppm of ethanol.

4.1.3.2 SnO_2 thick film

The sensor based on SnO_2 thick film was exposed to ethanol vapor with the concentrations of 50, 200, and 1000 ppm at the temperature of 200–350°C. The sensing characteristics of the sensor were similar to that of MoO_3 thick film. The resistance in air decreased with increasing temperature. Fig. 4.5 shows the sensor response of the SnO_2 thick film sensor as a function of the operating temperature. It was observed that the sensor response was highest at the operating temperature about 250°C. The sensor response was 6.3, 9, and 16.3 for the ethanol concentration of 50, 200, and 1000 ppm, respectively.

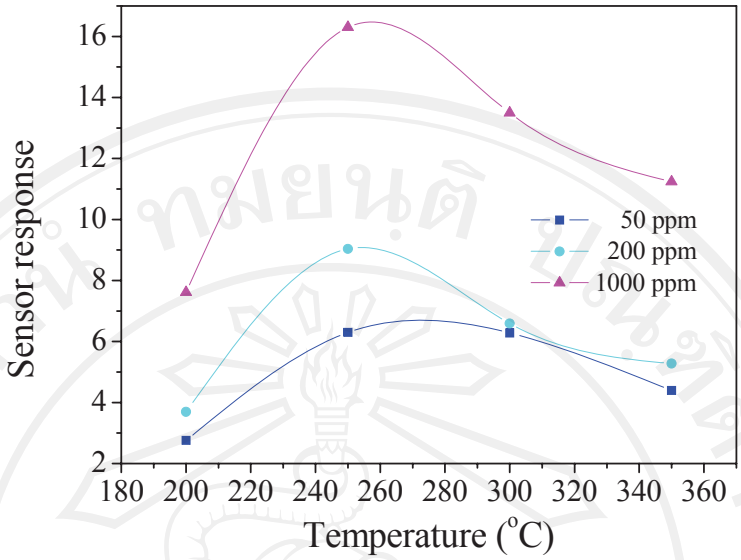

Figure 4.5 Sensor response of SnO_2 thick film as a function of temperature.

4.1.3.3 SnO_2 nanowires beaded nanoparticles

The sensor based on SnO_2 nanowires beaded nanoparticles was exposed to ethanol vapor with concentrations of 50, 100, 200, 500, and 1000 ppm at 240–360°C. The resistance in air as a function of the temperature was similar to that of SnO_2 thick film. The response and recovery curve and sensor response of the sensor for various ethanol concentrations were shown in Fig 4.6. It was observed that the response time decreased but the recovery time increased when the ethanol concentration increased. The sensor response of the sensor gradually increased as function of the operating temperature to reach the maximal value of 13.5, 27.8, 43.2, 81.2, and 104.3 for ethanol concentration of 50, 100, 200, 500, and 1000 ppm, respectively, at 340°C and then decreased. In comparison, the sensor response was about 2, 5, and 6 times higher than that of SnO_2 thick film for 50, 200, and 1000 ppm, respectively.

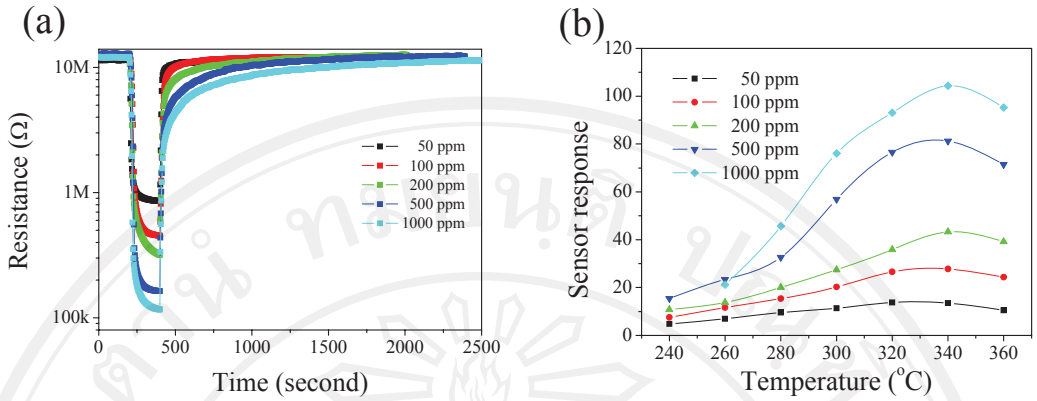

Figure 4.6 (a) Response and recovery curves of the sensor based on SnO_2 nanowires beaded nanoparticles at 340°C and (b) sensor response of the sensor as a function of temperature for various ethanol concentrations.

4.1.3.4 SnO_2 nanowires mixed nanodendrites

The sensor based on SnO_2 nanowires mixed nanodendrites was exposed to ethanol vapor with concentrations of 50, 100, 200, 500, and 1000 ppm at 240–360°C. The sensing characteristics were, generally, the same as that of SnO_2 nanowires beaded nanoparticles. However, the optimal temperature was shifted to higher temperature at 340–360°C. Furthermore, the sensor response was 22.0, 31.1, 52.8, 83.3, and 120 for ethanol concentration of 50, 100, 200, 500, and 1000 ppm, respectively, slightly higher than that of the SnO_2 nanowires beaded nanoparticles.

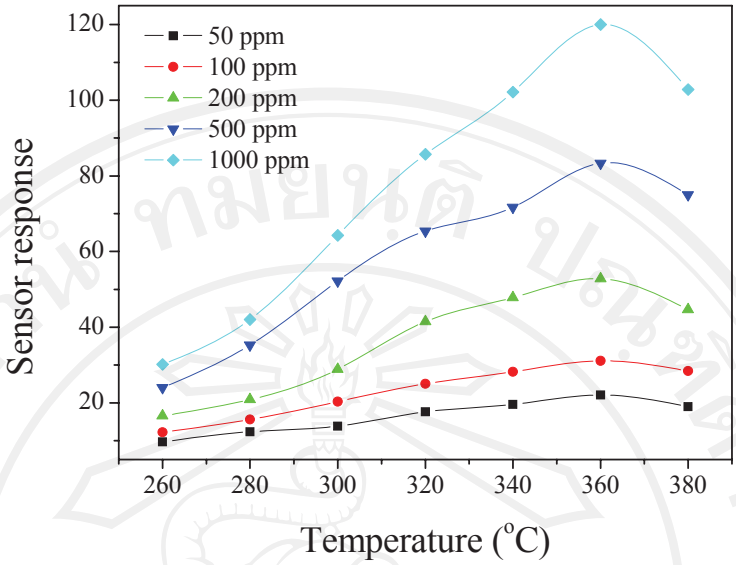

Figure 4.7 Sensor response as a function of temperature for SnO_2 nanowires mixed nanodendrites.

4.1.3.5 Au–impregnated SnO_2 nanowires

Three amounts of gold colloid, said 5, 10, and 15 µl, were used to functionalize the SnO_2 nanowires. Gold colloid of 5 µl was firstly dropped onto the SnO_2 nanowires and the sample was then heated at 300°C for 2 hours to remove any substance coming with gold colloid. After the sensing characteristics of the 5 µl dropped sample were carried out, another 5 µl of gold colloid was dropped to the old sample to make 10 µl dropped sample. The same fashion was performed for 15 µl dropped sample. The attachment of Au particles on the nanowires was shown in Fig. 4.8.

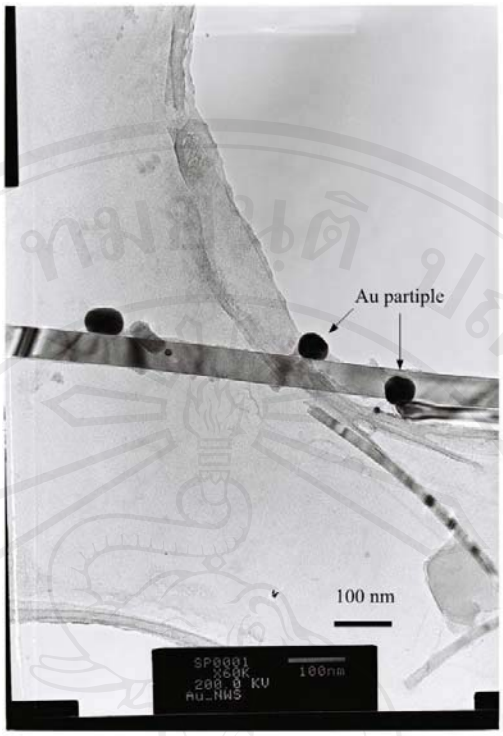

Figure 4.8 TEM image of Au–impregnated SnO_2 nanowires for 15 µl gold colloid.

The sensor based on Au–impregnated SnO_2 nanowires had the sensing characteristics differing from that of the pure one. Fig. 4.9 showed a typical resistance in air as a function of the temperature and response and recovery curve of the sensor. The resistance in air was about 29 MΩ at 240°C and increased continuously to about 36 MΩ at 300°C. Then the resistance decreased rapidly when the temperature increased, as seen in Fig 4.9a. Over recovery occurred at low temperature, as shown in the curves of 240°C and 260°C in Fig. 4.9b. The over recovery was eliminated when the temperature became high. The sensor response as a function of amount of gold colloid, for 1000 ppm ethanol at the optimal temperature (320°C), was shown in Fig. 4.10a. The sensor response started at about 93 for pure SnO_2 nanowires and

slightly decreased to 82 for 5 µl dropping. The sensor response enhanced to 138 when 10 µl of gold colloid was applied. The further dropping of gold colloid caused the decreasing of the sensor response. The sensor response for 10 µl dropped sensor as a function of the operating temperature was shown in Fig. 4.10b. The sensor response gradually increased as increasing of the operating temperature from 240–280°C and then rapidly increased to highest at 320°C. After that, the sensor response decreased rapidly for further increasing of the operating temperature. At the optimal temperature, the sensor response was 16.2, 26.5, 53.2, 80.5, and 138.5 for ethanol concentration of 50, 100, 200, 500, and 1000 ppm, respectively.

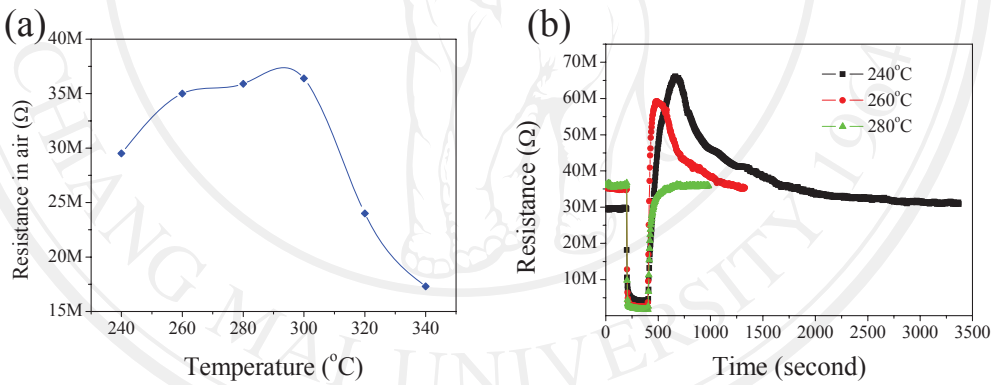

Figure 4.9 (a) A typical resistance in air as a function of temperature and (b) response and recovery curve for the sensor based on Au–impregnated SnO_2 nanowires.

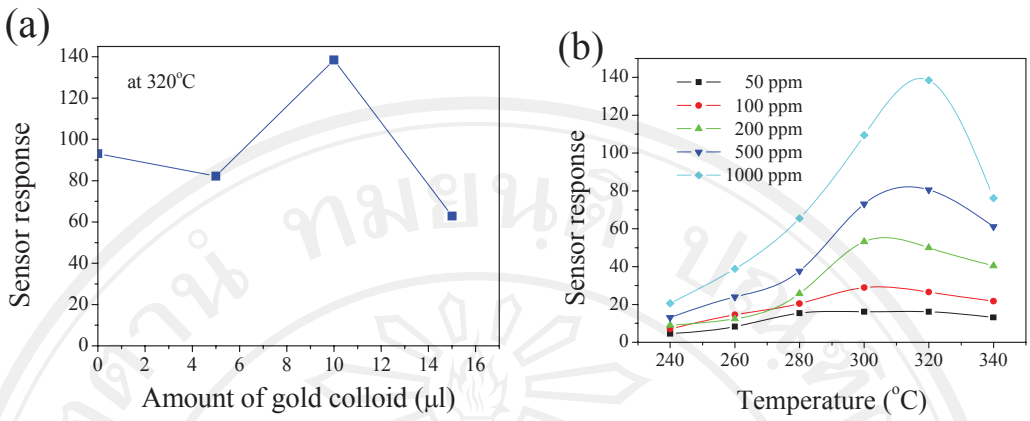

Figure 4.10 (a) Sensor response as a function of amount of gold colloid at 320°C at 1000 ppm of ethanol and (b) sensor response as a function of temperature for 10 µl gold dropped sensor at ethanol concentration of 50, 100, 200, 500, and 1000 ppm.

Furthermore, a sputtering technique was used to coat gold the SnO_2 nanowires. The sensor based on 60 s Au–coated SnO_2 nanowires was exposed to 1000 ppm of ethanol. For comparison, Fig. 4.11 shows the sensor response as a function of the operating temperature for pure, 5 µl gold dropping, 10 µl gold dropping, 15 µl gold dropping, and 60 s Au–coated SnO_2 nanowires. It can be seen that Au doping causes the optimal temperature shifted to lower temperature.

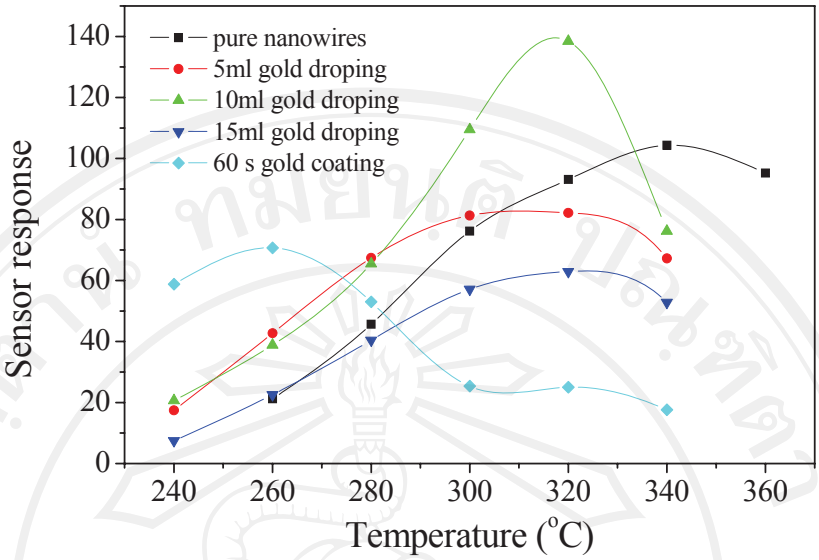

Figure 4.11 Comparison of the sensor response for pure and Au–impregnated SnO_2 nanowires to 1000 ppm of ethanol.

4.1.4 Gas sensing mechanism

The gas sensing mechanism of metal oxides has been clarified in previous works [77, 78]. At high temperature, the resistance of the sensing layer changes by adsorption and desorption of oxygen on the surface of the sensing layer. The carrier electrons are consumed by the formation of O^- and/or O^{2-} and this results in creation of the depletion layer leading to high barrier at inter–grain. Hongsith et al. [78] have formulated a relation which explains the sensor response of metal oxide gas sensors in functions of gas concentration, catalytic effect, and nanostructure effect, which can be expressed as

$$S = \left(\frac{\Gamma_t k_{Eth}(T)(\sigma_0 \Phi(V_m / V_s))^b}{n_0} \right) \frac{D^2}{(D - 2L_d)^2} C^b + 1 \qquad (4.1)$$

where Γ_t is a time constant, $k_{Eth}(T)$ is the reaction rate constant, σ_0 is a number of oxygen ion per unit area, Φ is a ratio of surface area per volume of material (V_m), V_s is the system volume, n_0 is the electron carrier concentration of the sensor, D is diameter of nanowire, L_d is the Debye length indicating the depletion layer, C is gas concentration, and b can be referred to the adsorbed oxygen species on the metal oxide surface. The $b-$value close to 1 (0.5), the surface dominates by O^- (O^{2-}).

The catalyst, such as Au, Pd, and Pt, has an effect on the sensor response through the reaction rate constant. The nanostructures can improve the sensor response in the terms of the surface to volume ratio, Φ, involving to the density of adsorbed oxygen ion on the surface. In the case the size of nanoparticles or the diameter of nanowires is comparable to $2L_d$, the depletion layer is formed inside the nanoparticles or nanowires mainly. Consequently, the conductance of sensing layer is governed by surface conductance more than bulk conductance.

As seen in the results of ethanol sensing characterization, the sensor response of the sensor based on SnO_2 nanostructures was many times higher than that of SnO_2 thick film. The $2L_d$ of SnO_2 is estimated about 40 nm at 320°C [79], whereas the diameter of the SnO_2 nanowires was about 50–100 nm. This indicated that the sensor response was not governed by the depletion effect. Therefore, it could be explained in terms of the surface to volume ratio of the nanostructures. In addition to the effects of gold particles on the sensor response, the enhancement of the sensor response could

be contributed by the increase of chemical reaction rate due to the existence of gold particles on the surface of nanowires. In other words, the effect can explain through the chemical sensitization mechanism [42], in which gold particles activate the oxygen spill over on the SnO_2 surface. Moreover, the gold particles also caused the dissociation of the oxygen molecule into ionic form and molecular ionic into atomic ionic at low temperature. This is clearly seen in Fig. 4.9a that the resistance increased as increasing of the temperature in 240–300°C.

Besides, the response and recovery time were affected by gold particles. Normally, oxygen diffusion in metal oxides plays a role in the response and recovery curve [80]. At low temperature, diffusion coefficient is low, leading to long response and recovery time. The over recovery effect, as seen in Fig. 4.9b, could be caused by the imbalance of oxygen adsorption and desorption rate. The existence of gold particles resulted in high rate of the oxygen adsorption, due to the spillover effect, at early moment after air was introduced. The resistance recovered when the rate of adsorption and desorption became balance.

Furthermore, the b–values of the sensors based on pure and Au–impregnated SnO_2 nanostructures at the optimal temperature were determined by plotting $\log(S-1)$ against $\log(C)$ and fitting with linear relation. The b–values were in the middle between 0.5 and 1, as seen in Table 4.2. This suggested that both O^- and O^{2-} associated on the surface of the sensors at their optimal temperature.

Table 4.2 The b–value of the sensors.

Sensing element	b–value
SnO_2 nanowires mixed nandendrites	0.60
SnO_2 nanowires beaded nanoparticles	0.66
5 µl gold dropping SnO_2 nanowires	0.80
10 µl gold dropping SnO_2 nanowires	0.70
15 µl gold dropping SnO_2 nanowires	0.65

4.2 Array sensors

4.2.1 Fabrication of array sensors

Two array sensors were fabricated, based on commercial sensors [75] and developed sensors [81], respectively, for study in e–nose application. Some studies were carried out by using commercial e–noses (E–nose Pty Ltd., Australia [82]) for use in chemometric study. The first array sensor was composed of four Tagushi gas sensors, listed in Table 4.3. The array sensor was put in a box with holes and a fan allowing gas flowed through the sensors, as shown in Fig. 4.12. The electronic lines were used for power supply and signal outputs. The signals were amplified or attenuated before inputting to analog–digital converter (ADC–11, Pico tech. UK) which connects to computer for data recording. The array sensor was separated from electronic module for ease of use. Second array sensor was composed of four developed sensor based on MoO_3 thick film, SnO_2 nanostructures, Au–impregnated

SnO_2 nanostructures, and Pd–impregnated SnO_2 nanostructures, as shown in Fig 4.13. This array sensor was tested similarly for ethanol sensing characterization.

Table 4.3 Tagushi gas sensors.

Sensor	Target gas
TGS 2100	Air contaminants
TGS 2602	Air contaminants
TGS 2611	Methane
TGS 2620	Alcohol, organic solvent vapor

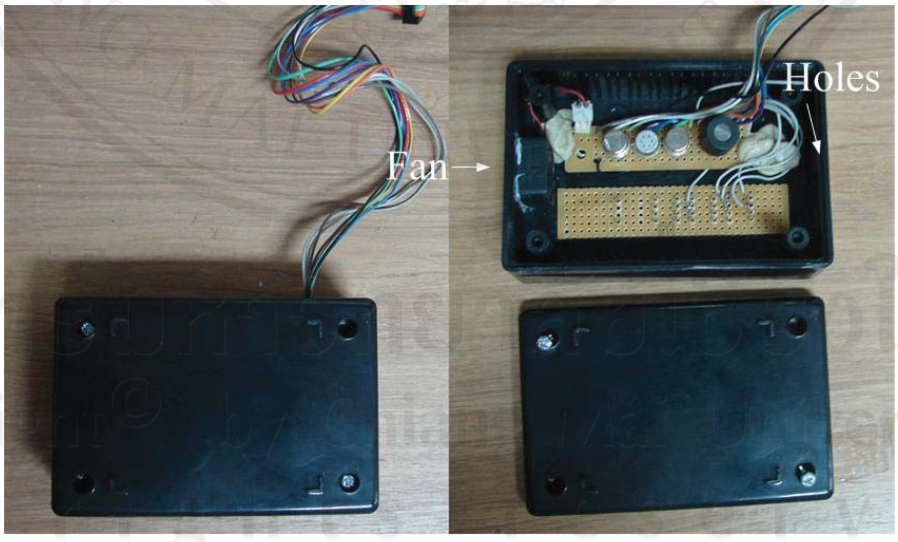

Figure 4.12 Box of the array sensor based on commercial sensors with a fan and holes.

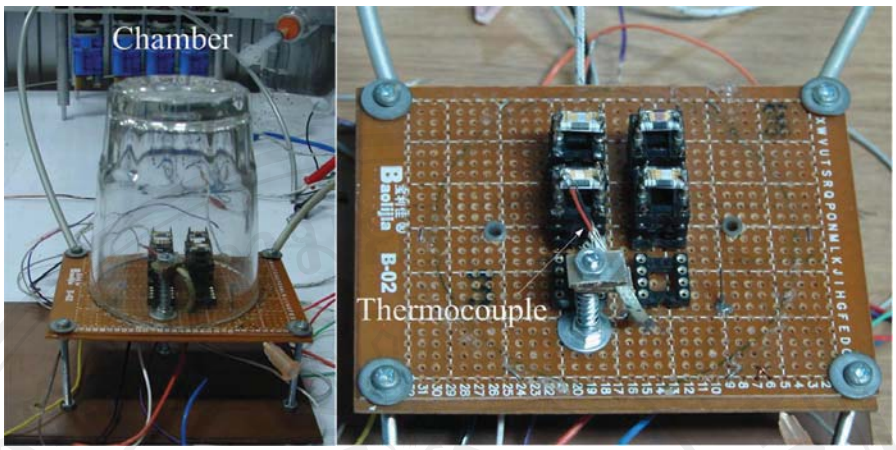

Figure 4.13 The developed array sensor.

4.2.2 Discrimination of vapors using array sensor

The signals from the array sensor are usually written as a matrix which number of column and row depends on the number of sensor and the taken sample, respectively. More than one point in the time profile of the signals can be taken into the matrix. The data from some sensors can be removed if it does not assist the e–nose performance. Therefore, two processes will be used to manage the signals and to obtain the classification or differentiation of samples.

Feature extraction: This process is used to extract useful information from the signals of the sensors or to remove the signal of some sensor which is not useful for classification in a specific task. There are many methods used for this purpose, depending on the criteria used, such as step wise – discriminant analysis (Step–LDA) which use the separation between groups as a criterion [83]. Other criteria can be used, for example prediction error, distance measure, or information content.

Pattern recognition (PR) methods: The most popular methods of PR data analysis are principal component analysis (PCA) [84], linear discriminant analysis (LDA), and artificial neuron networks (ANN) which will be briefly introduced in this section. The principal characteristics of these methods are summarized in Table 4.4. The basic calculation of PCA and LDA can be seen in Appendix B and C. The supervised method needs to know the class of the input data to generate a model for classification. Then an unknown data is used as a test data for the model. The non–supervised method does not need to know the class of the input data but learns the difference of classes automatically from the response vectors. A parametric technique is based on the assumption that the senor data can be explained by a probability density (PDF) like normal distribution, while a non–parametric technique is applied in general. PCA is, a non–supervised linear technique, used to reveal groupings among sets of classes. PCA reduces the complexity of the data set, from the initial n–dimensional space to a few dimensions, (significant principal components, PCs) which is used to display the graphical separation among classes. LDA is a supervised method which calculates the discriminant functions used for classification. Similar to PCA, LDA can also generate the graphical separation among classes using two or three first dimensions. ANN can be both supervised and non–supervised method for analyzing in complex and non–linear systems.

Table 4.4 Summary of the principal characteristics of pattern recognition methods [76].

Method	Learning	Linear	Parametric	Applications
PCA	Non–supervised	Yes	No	Feature extraction and classification
LDA	Supervised	Yes	Yes	Classification
ANN	Supervised/ non–supervised	No	No	Classification and quantitative mixture analysis

4.2.2.1 Classification among ethanol, hydrogen, and acetone by Bayesian analysis

Beside the methods mentioned above, Bayesian analysis [85] is a supervised and parametric method which can be used for classification or quantitative mixture analysis. To perform Bayesian analysis, the data of an analyzed gas for a sensor is, therefore, assumed to have a specific normal distribution. The normal distribution of the data of each analyzed gas is created by using mean and standard deviation. So the number of the normal distributions is equal to the number of analyzed gas times the number of sensors used.

In this work, a commercial e–nose of four sensors, S_1, S_2, S_3, and S_4, was used to measure the responses of ethanol, hydrogen, and acetone for chemometric study. The responses of 35 samplings for each gas were transferred to a spread sheet in

Excel^{TM}. The responses of S_1, S_2, and S_4, were divided by that of S_3 to eliminate the concentration dependence of the response. Hence, the responses of S_1, S_2, and S_4, were likely to exhibit as normal distribution. Mean and standard deviation of data for each gas and each sensor were calculated. These two values were used in normal distribution function, NORMDIST(x, mean, standard_dev, cumulative), in Excel^{TM}. The actual distribution and the representative distribution of data for each sensor were shown as histogram and normal distribution in Fig. 4.14. These normal distributions acted as database for classification of unknown samples. To classify an unknown sample to be ethanol, hydrogen, or acetone, the likelihood of the unknown sample was calculated by following steps. Supposed that the response matrix of the unknown after divided by that of S_3 is [x_1, x_2, x_4] and the likelihood of the unknown to be ethanol, hydrogen, acetone, and none of them, are represented by $Pr_i(x_i|E)$, $Pr_i(x_i|H)$, $Pr_i(x_i|A)$, and $Pr_i(x_i|N)$, respectively, for S_i.

$$Pr_i(x_i|C)=NORMDIST(x_i, mean\_x_i(C), standard\_dev\_x_i(C), cumulative) \quad (4.2)$$

$$Pr_i(x_i|N)=0.9(max_i-min_i) \quad (4.3)$$

where, i=1, 2, and 4, $mean\_x_i(C)$ is the mean of data in class C for S_i, $standard\_dev\_x_i(E)$ is the standard deviation of data in class C for S_i, max_i is the maximum value of S_i, and min_i is the minimum value of S_i. Vice versa, the likelihood of ethanol to be the unknown is represented by Pr(E|X).

$$Pr(E \mid X) = \frac{Pr(X \mid E)P(E)}{Pr(X \mid E)P(E) + Pr(X \mid H)P(H) + Pr(X \mid A)P(A) + Pr(X \mid N)P(N)} \quad (4.4)$$

Where, Pr(X|E), Pr(X|H), Pr(X|A), and Pr(X|N) are the likelihood of the unknown to be ethanol, hydrogen, acetone, and none of them, respectively. P() is the prior likelihood of each class. The numbers of step to calculate the likelihood of a class for a given unknown depend on the number of the sensor used. At first step of calculation, P() of all classes are equal. At second step, the likelihood of the class resulting from first step is used as P() of that class. The same fashion will be used until the final step. The unknown, X, will be assigned to the class that has maximum likelihood. Table 4.5 shows the final result of calculation. The result showed that the unknown could be assigned to be hydrogen with 78.1% of likelihood. However, it also had a chance to be acetone with 21.9% of likelihood. As seen in Fig 4.14, data of gases overlapped to each other, leading to only 82.5% of classification correction.

Table 4.5 Spread sheet of the calculation result.

	Ethanol		
	S1/S3	S2/S3	S4/S3
mean	9.83	2.65	8.22
sd	0.78	0.16	0.58
	Hydrogen		
	S1/S3	S2/S3	S4/S3
mean	12.41	2.33	10.20
sd	1.44	0.26	1.18
	Acetone		
	S1/S3	S2/S3	S4/S3
mean	11.69	3.02	9.48
sd	1.44	0.23	1.05

Sensor	MAX	MIN	Pr(data|none)	within training data
S1	16.46	8.60	0.10	0.01
S2	3.61	1.66	0.54	0.05
S4	13.70	7.32	0.12	0.02

	Sample	Ethanol	Hydrogen	Acetone	None	Classify
	E	4.80%	59.82%	35.37%	0.01%	H
	E	74.48%	16.53%	8.99%	0.01%	E
	E	85.91%	8.34%	5.74%	0.00%	E
	E	94.60%	3.38%	2.01%	0.00%	E
	H	0.00%	97.45%	0.00%	2.55%	H
	H	0.00%	99.86%	0.00%	0.14%	H
	H	0.00%	99.91%	0.00%	0.09%	H
	H	0.00%	99.84%	0.00%	0.16%	H
	A	0.00%	22.72%	77.27%	0.01%	A
	A	0.00%	11.20%	88.78%	0.02%	A
	A	49.41%	13.95%	36.63%	0.01%	E
	A	0.00%	7.84%	92.14%	0.01%	A

Prediction				
	S1	S2	S3	S4
unknown	0.20	0.04	0.02	0.18

		Pr(data|E)	Pr(data|H)	Pr(data|A)	Pr(data|none)	Sum
S1/S3	13.18	0.00	0.24	0.16	0.01	0.41
S2/S3	2.71	2.33	0.53	0.67	0.05	3.58
S4/S3	11.51	0.00	0.18	0.06	0.02	0.26

		Pr(E|data)	Pr(H|data)	Pr(A|data)	Pr(none|data)	SumProd
	Prior	0.25	0.25	0.25	0.25	0.10
	S1	0.00	0.58	0.39	0.03	0.57
	S2	0.00	0.54	0.46	0.00	0.13
Result	S4	0.00%	78.09%	21.88%	0.03%	

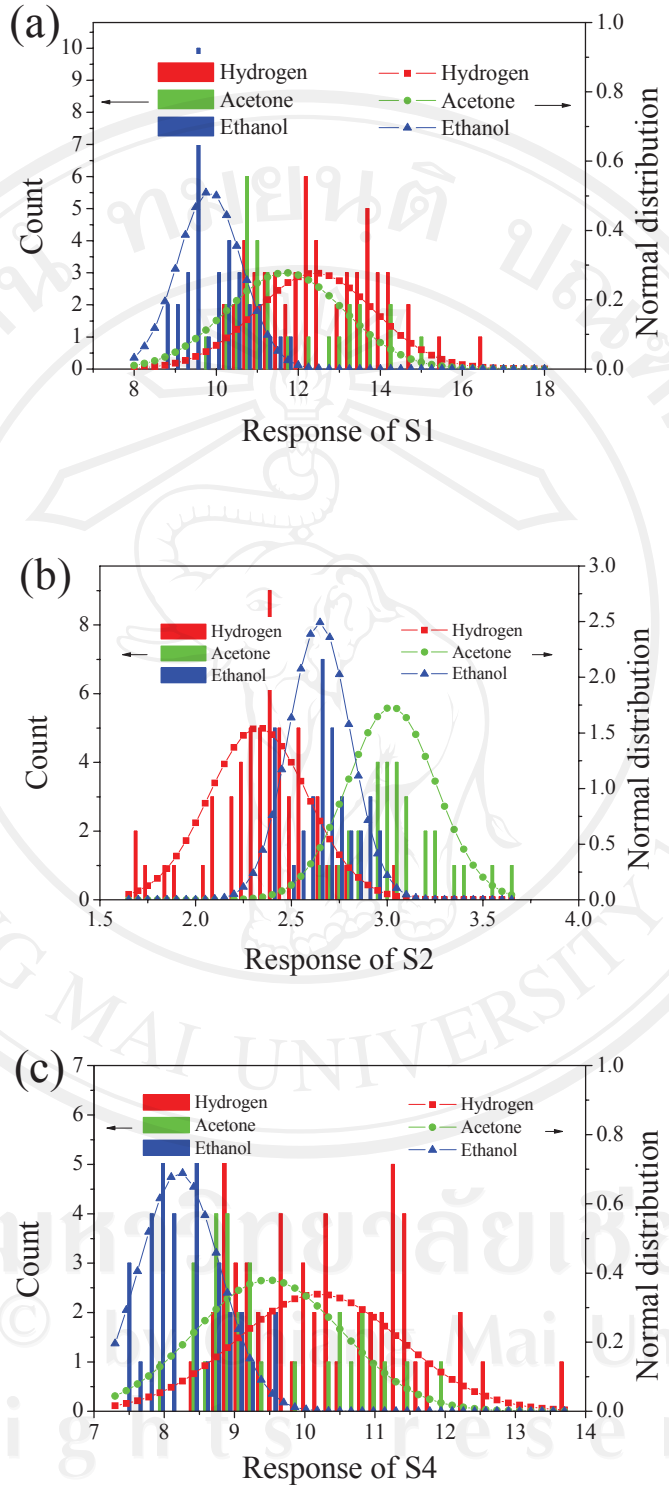

Figure 4.14 Histograms and distributions of data for (a) ethanol, (b) hydrogen, and (c) acetone.

4.2.2.2 Discrimination among gases with PCA assisted by row–wise standardization technique

This task was carried out by using a commercial e–nose of five sensors to analyze three concentrations of acetone, ethanol, iso–propanol, methanol, and toluene. The row–wise standardization, which is used to eliminate the concentration dependence of the response, will be effective if the responses of sensors have a linear relationship to each other for a gas, see more details in Appendix A. Therefore, the response of each sensor for ethanol was plotted against that of the S_1, corresponding to before and after base–line subtraction as shown in Fig. 4.15a and b. The results showed that it was worth to apply the row–wise standardization to this data. Fig. 4.15c shows the row–wise standardized data for all gases, where a unique response pattern of each gas can be seen. The row–wise standardized data was analyzed with PCA by using PLS toolbox performed in Matlab©. Row–wise standardization technique remarkably improved the graphical separation of the classes of samples due to a unique linear relationship between sensors for a gas. Fig. 4.16 compares the PCA score plot on the original data and the row–wise standardized data. With original data, PCA could ambiguously separate the gases and samples of the same gas, especially ethanol, were spread widely and separated because of concentration dependence of data. The best separation view is shown in Fig. 4.16a. By applying the row–wise standardization technique to make concentration independence data, PCA could group samples of each gas together, leading to definite separation among the gases as shown in Fig. 4.16b.

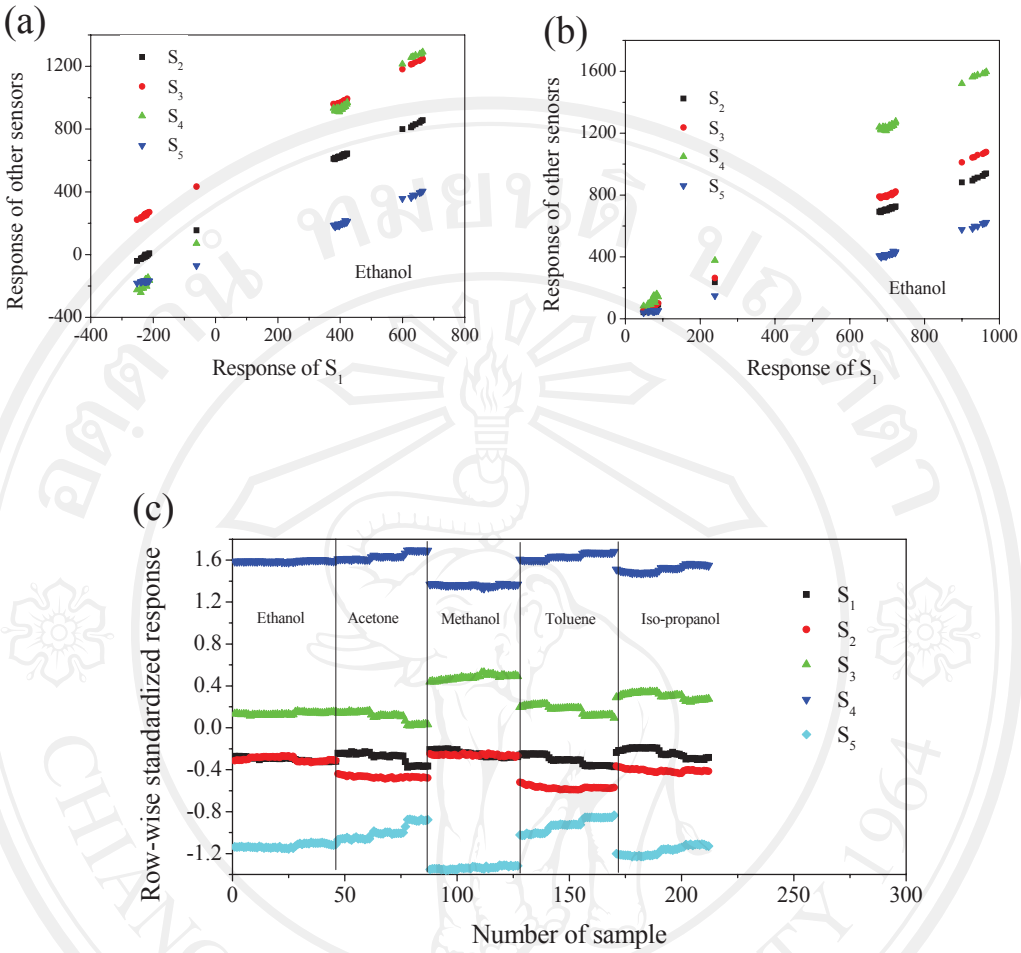

Figure 4.15 Plot of the responses of sensors against that of S_1; (a) before and (b) after baseline subtraction. (c) Row–wise standardized data showing a unique response pattern for each gas.

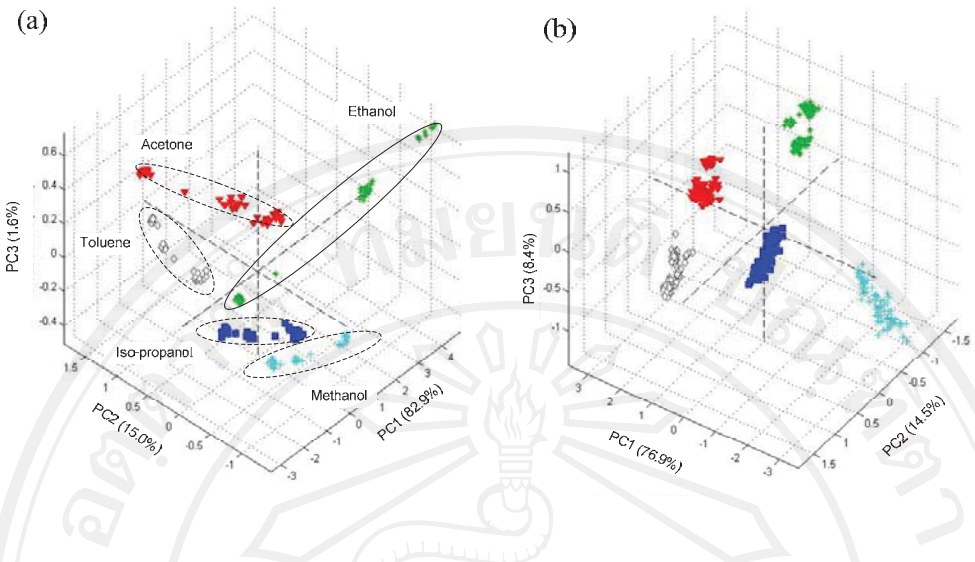

Figure 4.16 PCA score plot on (a) original data and (b) row–wise standardized data of the first three components with 99.5% and 99.8% of total variance, respectively.

4.2.2.3 Classification of gasoline and ethanol blended gasoline

Nowadays, Thai government allows gasoline blended with 10, 20, and 85 percent of ethanol (E10, E20, and E85, respectively) in commercial use. These blended gasolines are called "gasohol" and their price is cheaper than the normal gasoline. Some trader can defraud by switching the gasohol to be the gasoline for higher price. Moreover, the gasoline can be adulterated with small amount of industrial solvents such as kerosene or used lubricants. The adulterated gasoline would cause the engine knock for long term use. It is worthwhile to establish a system to monitor the quality of fuel. To study the possibility of using an array sensor in such purpose, the developed array sensor, based on commercial sensors, was used to classify among gasoline 91 (B91) and gasohol (E10, E20, and E85) from PTT Public Company Limited. Ten samplings of each vapor were recorded. A typical

response of the array sensor was in Fig. 4.17a. Points at saturation period in the response were averaged and used to analyze with LDA, performed in Matlab©. The response patterns of all gases were shown in Fig. 4.17b. LDA result showed that samples were separated definitely into three groups. Samples of E10 and E20 were grouped together at the middle between E85 and B91 samples, as seen in Fig. 4.17c. The arrow in Fig. 4.17c shows the trend of ethanol content in gasoline.

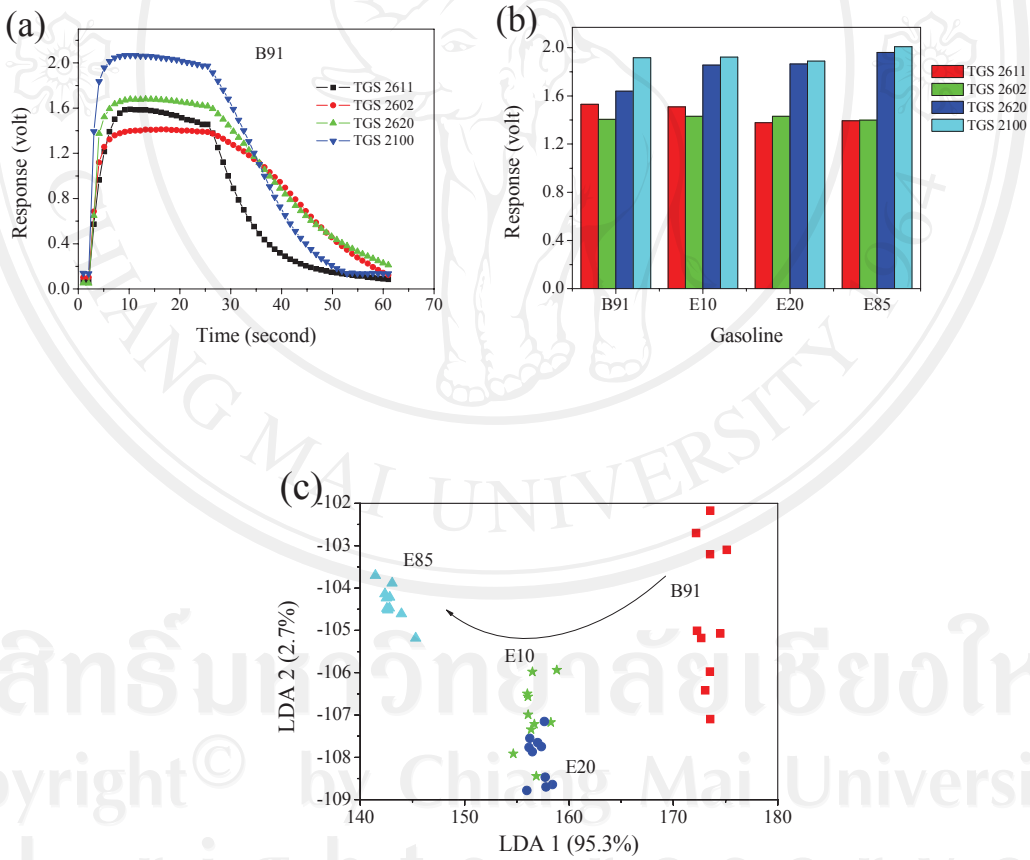

Figure 4.17 (a) A typical response of array sensor to gasoline 91 (B91), (b) average response pattern of B91, E10, E20, and E85, (c) LDA score plot of two first components with 98.0% of total variance.

4.2.2.4 Classification ability of the array sensor based on developed sensors

The array sensor based on developed sensors was exposed to ethanol and acetone with concentrations of 50, 100, and 200 ppm at the operating temperature of 320°C. Each concentration was sampled twice. To see the response pattern of the array sensor, the typical sensor responses of the array sensor were plotted against the concentration of ethanol and acetone, as shown in Fig. 4.18a and b. It can be seen the different pattern of the responses between ethanol and acetone in each concentration but not obviously. However, PCA score plot showed that the data points separated into two groups obviously, as shown in Fig. 4.18c. The arrows in Fig. 4.18c showed the trend of the concentration of each substance in the space of the reduced dimension. In addition, the relationship or redundancy among sensors was shown in PCA loading plot, Fig. 4.18d. The points in the plot were separated to each other, which meant that each sensor gave a specific response for the analyzed gases. This suggested that the array sensor based on MoO_3 thick film, SnO_2 nanostructures, Au–impregnated SnO_2 nanostructures, and Pd–impregnated SnO_2 nanostructures, could be developed as a device for e–nose application.

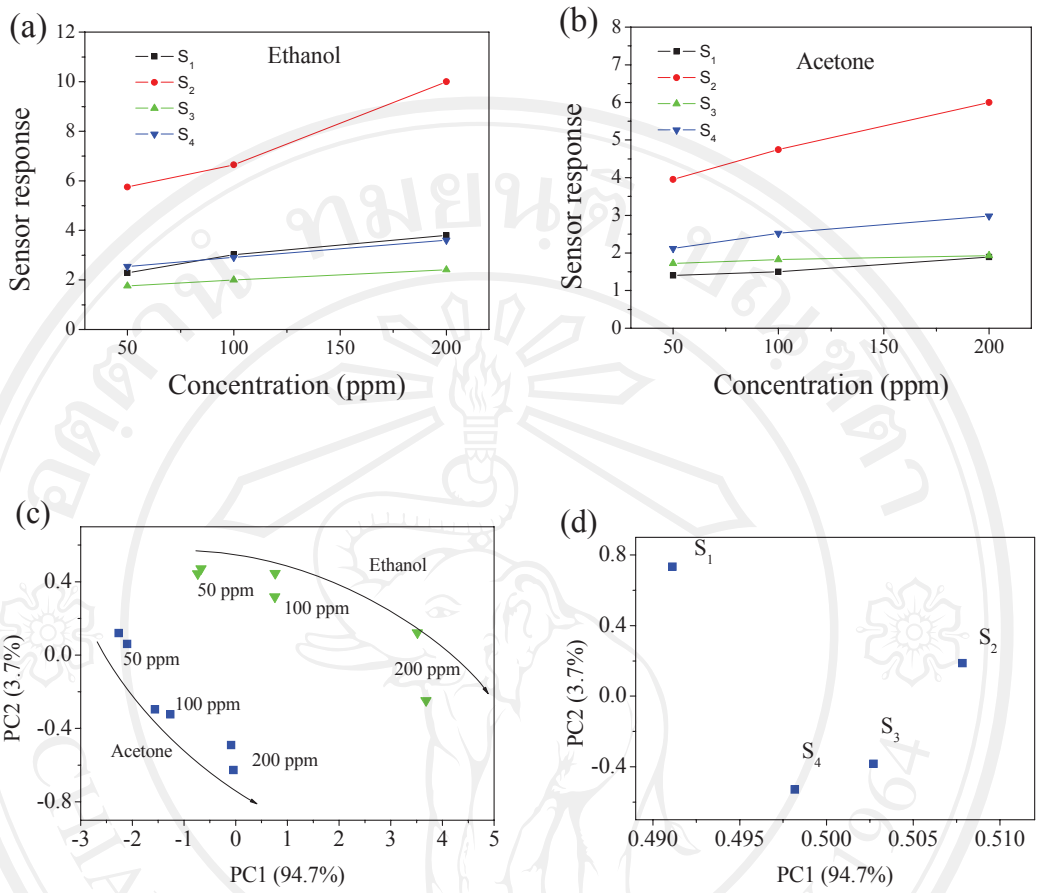

Figure 4.18 Typical sensor response of the array sensor as a function of concentration: (a) ethanol and (b) acetone. S_1, S_2, S_3, and S_4 refer to MoO_3 thick film, SnO_2 nanostructures, Au–impregnated SnO_2 nanostructures, and Pd–impregnated SnO_2 nanostructures, respectively. (c) PCA score plot and (d) PCA loading plot of data with two first components holding 98.4% of total variance.